Supplemental information for:

# Electron-beam evaporated silicon as a top contact for molecular electronic device fabrication

**Rajesh Kumar,**[a]**Haijun Yan**[b], **Richard L. McCreery**[a,b], **and Adam Johan Bergren\***[b]
[a] *Department of Chemistry, University of Alberta, Edmonton, Alberta, Canada.*
[b] *National Institute for Nanotechnology, Edmonton, Alberta, Canada.*
Fax: 780 641 1601; Tel: 780 641 1762; E-mail: Adam.Bergren@nrc.ca

## Introduction

This document contains supplemental supporting data for the above paper, including electronic characteristics and attenuation plots, Raman peak assignments for nitroazobenzene (Table S-1), and Raman, conductivity vs. temperature, UV/vis, and Kelvin probe characterizations of evaporated Si films.

**Table S-1.** Peak assignments for Raman bands observed in Figure 1[1-3].

| Peak (cm$^{-1}$) | Assignment |
|---|---|
| 1103 | Ph-NO$_2$ stretch |
| 1137 | Ph-N$_2$ stretch |
| 1188 | CH bend |
| 1337 | NO$_2$ stretch |
| 1398 | N$_2$ stretch |
| 1446 | N$_2$ stretch |
| 1589 | C=C ring stretch |

## Experimental

Raman spectroscopy was used to characterize the phase of e-beam evaporated Si (e-Si) film. 30 nm Si films were evaporated via electron beam evaporation onto different substrates, including thermally oxidized Si wafers, quartz, and PPF (pyrolyzed photoresist film- see main text). Raman spectra were recorded using a Thermo/Nicolet Raman microscope with a 5-10 second exposure time on a CCD detector and excitation wavelength of 532 nm. All the spectra (unless otherwise specified) were recorded with low enough laser power densities to avoid any observable changes to the Si spectrum due to radiant heating.

The temperature dependence of the resistivity was determined by depositing a 30 nm film of Si across a gap defined by patterned gold electrodes on a thermally oxidized (300 nm oxide thickness) Si wafer. The length of the gap was 0.5 mm and the span was 10 µm. Using these dimensions, the measured current at +1 V was used to convert first to a resistance and then to a

resistivity value. The value of the resistivity at room temperature determined in this way (2276 $\Omega$ cm) is in reasonable agreement with an independent measurement of the resistivity of 30 nm Si films on quartz at room temperature using a Lucas Labs Signatone Pro4 measurement system (3300 ± 300 $\Omega$ cm). The temperature was varied using a Janis ST-500-1 cryogenic probe station[4, 5] with liquid $N_2$ coolant and a resistive stage heater; these measurements were carried out while the sample was under a vacuum of ~$10^{-6}$Torr.

UV/visspectra were recorded in transmission mode using a Perkin-Elmer Lambda 900 spectrometer. The spectrum for a 30 nm film on quartz was referenced to an uncoated quartz sample.

Kelvin probe measurements were carried out using an SKP5050 from KP Technology in laboratory ambient[6]. A 2 mm diameter gold tip was scanned across the surface of a sample of PPF that was half-coated with a 30 nm layer of evaporated Si. Thus, the work function of the uncoated PPF was directly compared to that for the Si film on PPF. To calibrate the work function of the gold tip, immediately prior to each measurement the work function for a freshly cleave highly oriented pyrolytic graphite (HOPG) sample was determined. HOPG has a well-defined work function of 4.475 eV in air[7].

## Results and Discussion

### *Sample Aging*

Figure S-1 shows a plot of $J_{1.5V}$ as a function of time for a PPF/AB(3.8)/Si(30)/Au(20) sample. After 15 h, the value of $J$ is 35% (1.0 V) and 25% (1.5 V) of the initial value. While we do not currently understand this phenomenon, the effect is likely attributable to oxidation of Si, which changes its carrier density, reduces its density of states, and/or reduces the effective junction area. Although there are several strategies that might be employed to reduce or eliminate this effect (including hydrogen gas in the chamber during deposition or sealing the devices in an inert atmosphere), we have taken care to measure devices immediately upon removal from the chamber to ensure consistent results (e.g., see Figure S-2 for batch-to-batch reproducibility for five different runs).
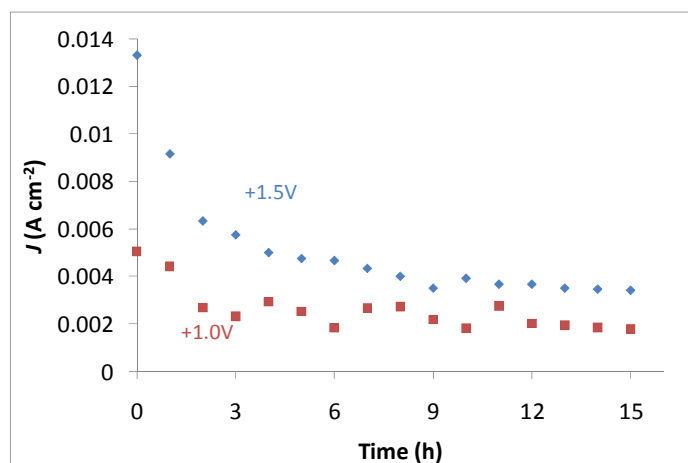
**Figure S-1.** Decrease in the current density measured at 1.0 and 1.5 V as a function of time for a PPF/AB(3.8)/Si(30)/Au(20) junction.

### *Supplemental Reproducibility Plots*

Figure S-2 shows all 8 junctions used to construct the plot in Figure 2 of the main text overlaid in a single plot. As shown, one junction out of 8 had an unstable *J-V* curve, , which was the basis for exlusion (i.e., the yield for this set of junctions is 7/8). Figure S-3 shows a plot for five different fabrication runs to produce PPF/AB(3.8)/Si(30)/Au(20) junctions. The value of *J* falls within a factor of 1.6 for all curves, illustrating that good reproducibility was obtained.
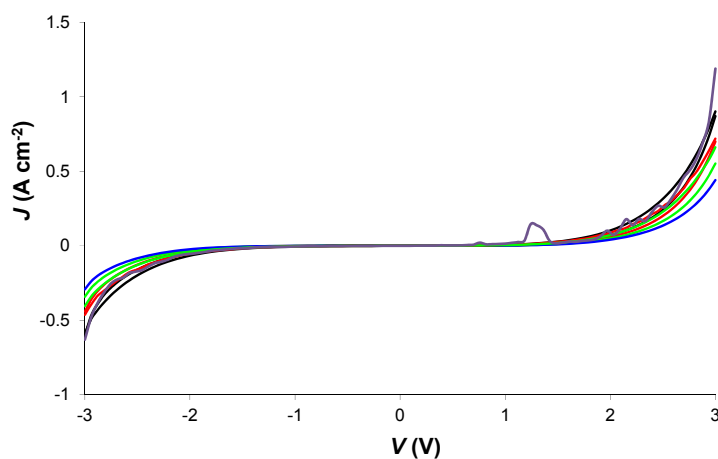


**Figure S-2.** Overlay of all 8 *J-V* curves from Figure 2 of the main text.
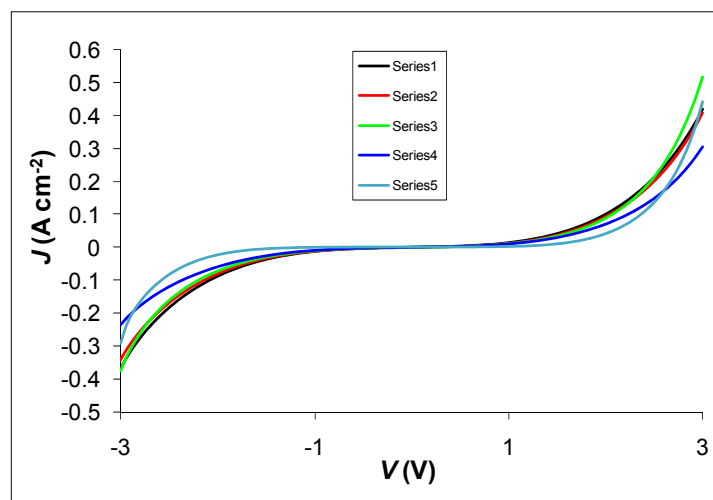
3

**Figure S-3.** Overlay of five *J-V* curves for PPF/AB(3.8)/Si(30)/Au(20) molecular junctions to show the level of reproducibility from batch-to-batch. The value of *J* at +3 V spans a factor of 1.6 (i.e., $J_{+3V}$ for Series 3 is 0.46, while that for Series 4 is 0.28).

### *Supplemental Attenuation Plots, Arrhenius Plots, and J-V Curves*

Figure S-4 shows attenuation plots for junctions containing azobenzene (AB) for the data in Fig. 3 of the main text using both the current density at different voltages (Fig. S-4A) and the low voltage resistance (Fig.S-4B) determined by the inverse slope of the current-voltage (*i-V*) curve. This analysis yields a value for β of 2.2-2.6 nm⁻¹ and an extrapolated contact resistance (determined from the intercept of the Figure S-4B at zero thickness) of 4.8 Ω. Figure S-5A shows J-V curves and Figure S-5B shows the corresponding attenuation plots for junctions containing NAB. As shown, the value of β determine from these data is 2.3-2.9 nm⁻¹. Figure S-6 shows Arrhenius plots for two junctions, illustrating the similar behaviour is observed. Figure S-7 shows the attenuation plot for junctions made using alkanes, yields a β = 9.9 nm⁻¹. Figure S-8 shows an overlay of junctions with equal thicknesses (determined by AFM) but both aromatic (AB) and aliphatic (C8) structures.
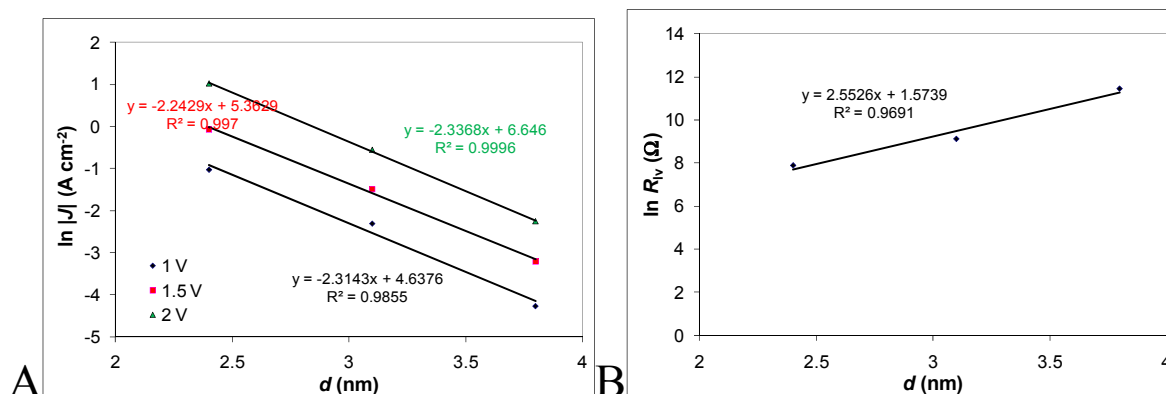
**Figure S-4.** (A): attenuation plot for the data in Fig. 3 of the main text. The value of β determined from these plots is 2.25 – 2.34 nm$^{-1}$. (B): attenuation plot for Fig. 3 of the main text calculated using the low voltage (±0.1 V) resistance values. The value of β is 2.55, and the extrapolated contact resistance is 4.8 Ω.
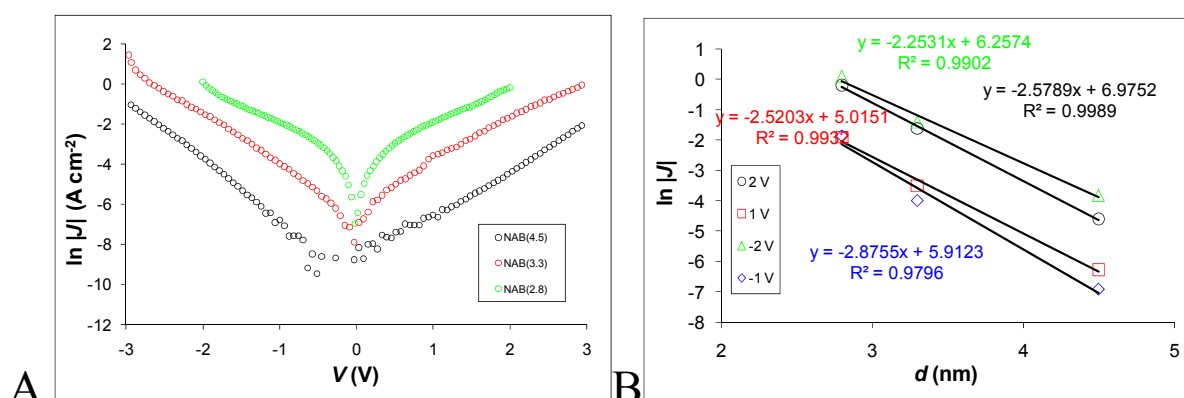


**Figure S-5.** *J-V* curves for a series of NAB junctions with different thicknesses (A) and the corresponding attenuation plot (B) showing β = 2.3-2.9 nm$^{-1}$.
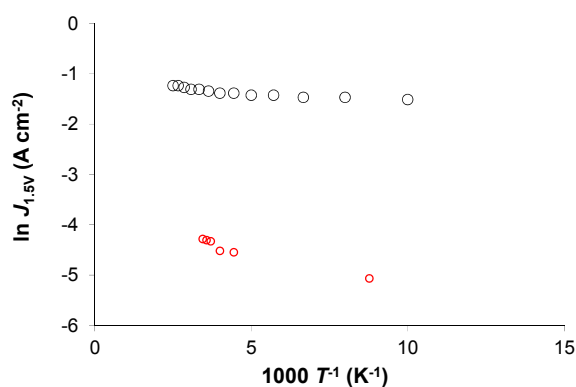


**Figure S-6.** Overlay of Arrheius plots for two junctions examined for temperature dependence. The black circles represent the plot shown in Figure 4 of the main text (for AB(3.8 nm), while the red circles are for a PPF/NAB(4.5nm)/Si junction. The Arrhenius slopes for these two junctions above 200K are 8 meV (black circles) and 12 meV (red circles), respectively.
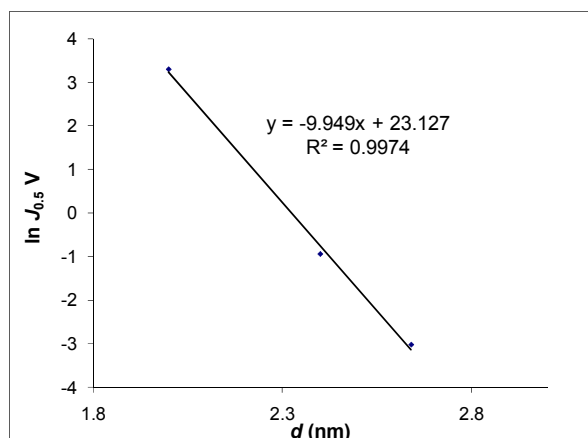
5

**Figure S-7.** Attenuation plot for the data in Figure 6 of the main text ($\beta = 9.9$ nm$^{-1}$).
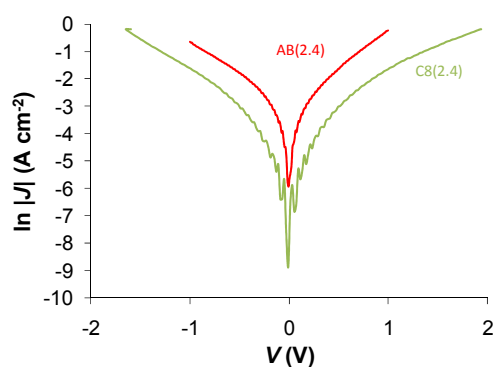


**Figure S-8.** Overlay of *J-V* curves for the same thickness of an aromatic (red curve) and aliphatic (green curve) molecular layer, showing that the junction made using the aromatic layer is ~5-7 times more conductive than the junction made with a saturated structure.

### *Raman Characterization of Evaporated Si Films*

The blue curve in Figure S-9Ashows Raman spectra for an evaporated Si film on Si/SiO$_2$. This spectrum shows a broad band centered ~470 cm$^{-1}$ and a sharp peak at 520 cm$^{-1}$. Amorphous Si typically shows a Raman band[8-10] between 470 and 480 cm$^{-1}$, indicating the sample contains non-crystalline Si. The high intensity and sharp peak at 520cm$^{-1}$ is attributed to the crystalline Si in the underlying substrate and this peak also appears in an uncoated sample (spectrum in black). Finally, SiO$_2$ typically shows a Raman band[11]near 440 cm$^{-1}$.

To eliminate the contribution from the crystalline Si substrate, Raman spectra for an evaporated Si film on quartz were also obtained, as shown in Figure S-9B.The black curve is the

spectrum for the uncoated quartz substrate, which shows a broad band around 440 cm$^{-1}$, which is typical for $SiO_2$[11]. On the other hand, the Raman spectrum for the 30 nm evaporated Si film on quartz shows a band at ~470 cm$^{-1}$, as shown in blue in Fig. S-9B.Again, this band is typical of amorphous Si[9, 10]. The band due to the Si film is clearly distinguishable from the $SiO_2$ band located at ~440 cm$^{-1}$ originating from the substrate (black spectrum in Fig. S-9B), indicating that the band at 470 cm$^{-1}$ is not due to silicon oxide. Finally, the absence of any peak at 520 cm$^{-1}$ in the blue spectrum suggests the absence of a significant crystalline Si component.

The Raman spectra in Figure S-9indicate that the evaporated Si films are amorphous in nature, and probably contain a small amount of oxide. One final test of the Si films was carried out by using a high laser power density of 60 mW/µm$^2$ (ten times higherlaser power relative to the other spectra in the Fig.S-9).The red spectrum shown in Fig. S-9Bshows that upon irradiating the sample with a higher laser power, a band near 500 cm$^{-1}$appears and the band for amorphous Si at 470 cm$^{-1}$decreases in intensity. The appearance of 500 cm$^{-1}$ peak can be understood by considering that a higher excitation laser power density can anneal the silicon film due to local heat generation, forming nanocrystalline Si, as reported in literature[12-15]. The position of this nanocrystalline Si peak varies from 500 to 519, depending on the size of the nanocrystals[16, 17]. This experiment shows that the as-evaporated Si film is amorphous, and that the contributions fromSiO$_2$or crystalline Siaresmall.
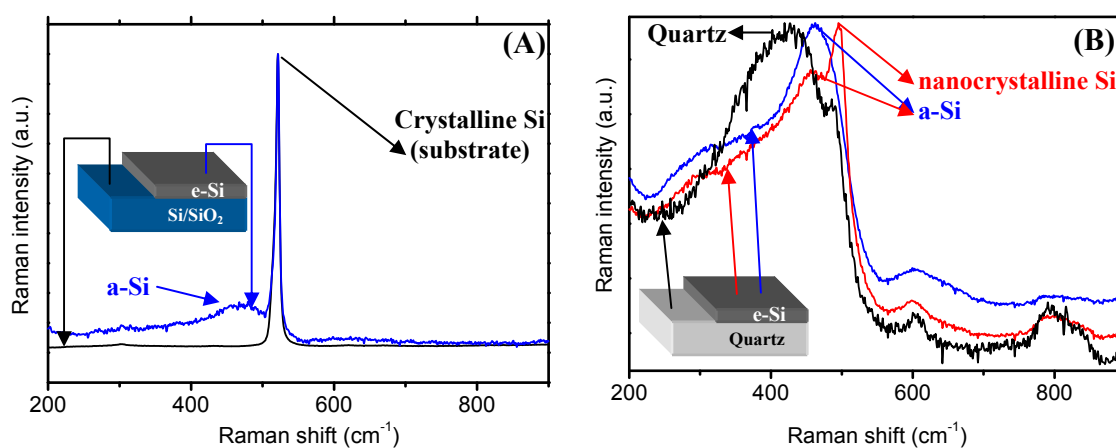


**Figure S-9.** Raman spectra from 30 nm thick e-beam silicon film on (A) Si substrate and (B) quartz substrate. Raman spectra from bare silicon and bare quartz substrates have also been shown for comparison in (A) and (B) respectively. Raman spectrum from a laser annealed spot (shown in red) on silicon film on quartz substrate is also shown in (B).

***Temperature Dependence of the Si Film Resistivity***

The resistivity (ρ) of a 30 nm film of evaporated Si on quartz measured at room temperature was 3300 ± 300 Ω cm. Because measurements of ρ as a function of temperature are often used to evaluate Si films, we have carried out measurements from 90 to 400 K. Figure S-10shows several plots of this data, including lnρ vs. $T^{3/2}$, lnρ vs. 1000 $T^{-1}$, and log ρ vs. log $T$. First, the linear portion in Figure S-10A below 200 K is consistent with impurity based scattering controlled conduction[18]. Atlower temperatures (on the left side of Figure S-10A), there is a transition to lattice-based scattering, which has a $T^{-3/2}$ dependence (visible in the plot in Figure S-10B). This indicates a high level of defects in our film, which is consistent with the amorphous nature determined using Raman spectroscopy. The Arrhenius plot in Figure S-10B shows a linear region at high temperatures, which indicates a change in the carrier concentration with temperature[18]. The values of the "barriers" calculated from this plot are consistent with literature values for polycrystalline or amorphous Si[18, 19].
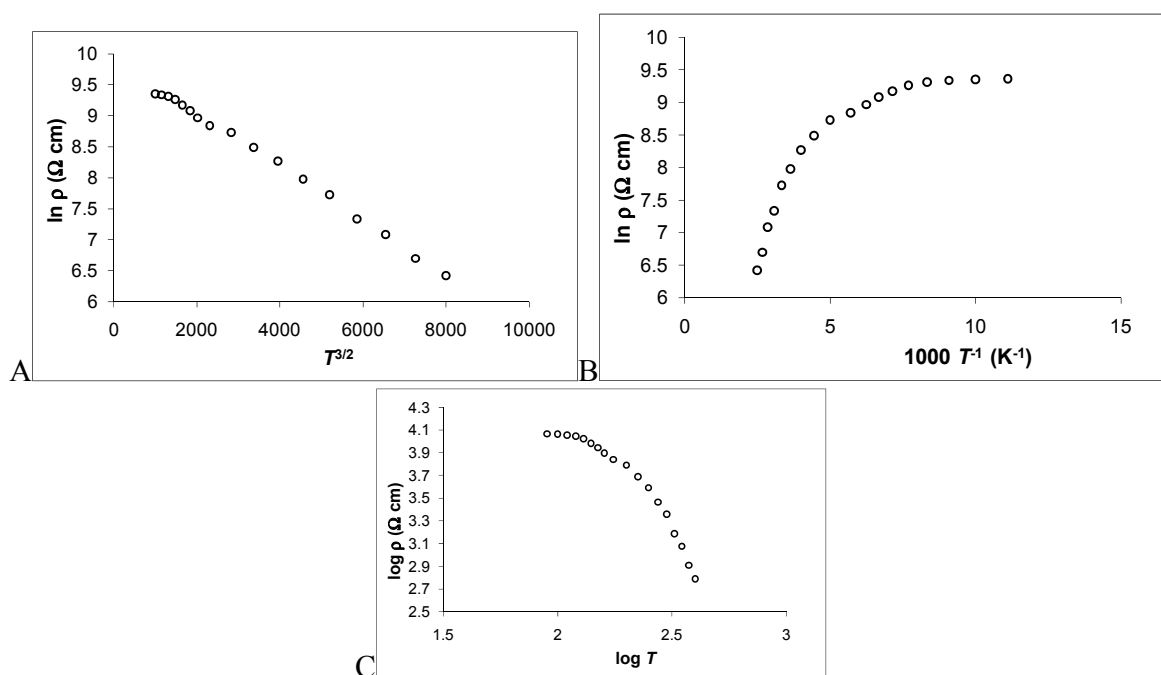


**Figure S-10.**(A): plot of the resistivity of a 30 nm Si film as a function of $T^{3/2}$. (B): Arrhenius plot showing a "barrier" of 90meV above 200 K and 8meVbelow 200 K. (C): log-log plot of resistivity versus $T$. All of the plots in this figure are consistent with polycrystalline or amorphous Si films reported in literature[18, 19].

### *UV/vis Characterization of Evaporated Si*

The UV/vis spectrum for a 30 nm Si film on quartz is shown in Figure S-11. This spectrum is consistent with that for an amorphous semiconductor[20]. Analysis of this data gave an optical gap of 1.1 eV, consistent with expectations for amorphous silicon. This adds to the other characterizations to show that evaporated Si films are amorphous and show many of the expected properties for a thin film of Si.
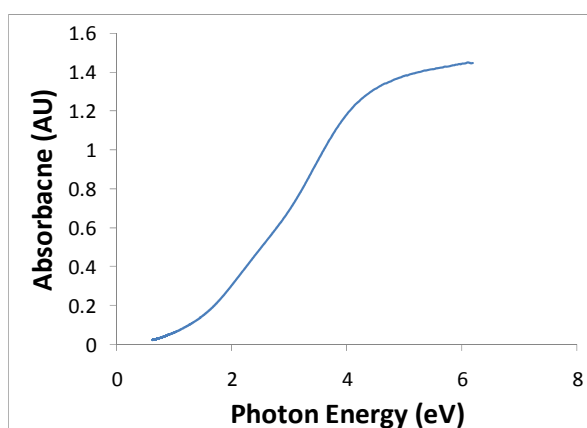


**Figure S-11.** UV-vis spectrum of a 30 nm Si film on quartz (referenced to quartz).

### *Kelvin Probe Characterization of PPF and PPF/Si*

Finally, we have measured the work function of a PPF sample half coated with a 30 nm evaporated Si layer using a 2 mm diameter tip. Figure S-12shows a plot of the measured work function versus position on the sample. In the area over the uncoated PPF, a work function of 5.0 ± 0.1 eV is measured, consistent with previous measurements of the PPF work function[6]. This drops to 4.2 eV over the area coated with Si, indicating a significant difference in the energy level of the Si contact. The sample was measured the same day it was removed from the vacuum chamber after coating half of the PPF with evaporated Si.
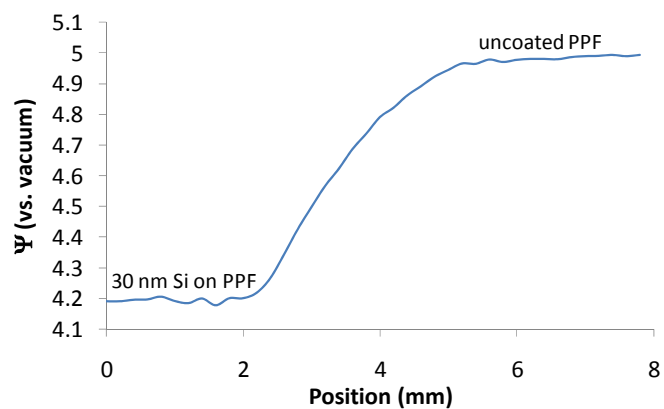
**Figure S-12.** Scanning Kelvin probe measurement on a sample coated with 30 nm of evaporated Si on half of the sample using a 1 mm tip. The profile was obtained by scanning across the boundary region to show the different in work function between the coated and uncoated areas.

**Supplemental Data Tables**

Table S-2 lists the yield and RSD values for the junctions studied in this work and Table S-3 contains molecular energy level values.

**Table S-2.** Yield and RSD for the junctions analyzed in this study. The values for the RSD are calculated based on the current density at +1.0 V unless otherwised noted. "Nonworking" junctions for yield calculation showed linear JV responses with very high current densities, indicative of direct PPF-Si contact.

| Sample | #Junctions | Yield | RSD |
|---|---|---|---|
| AB(2.4 nm) | 4 | 100% | 9% |
| AB(3.1) | 4 | 100% | 21% |
| AB(3.8) | 20 | 95% (19/20) | 16% |
| NAB(2.8) | 4 | 100% | 47% |
| NAB(3.3) | 4 | 75% (3/4) | 77% |
| NAB(4.5) | 4 | 100% | 14% |
| C8(2.0) | 8 | 63% (5/8) | 63% (0.1 V) |
| C8(2.4) | 8 | 100% | 25% |
| C8(2.6) | 8 | 100% | 8% |
| FL(2.0) | 4 | 100% | 7% (0.5 V) |
| Overall | 68 | 93% | - |

**Table S-3.** Values for molecular energy levels calculated from Gaussian'03 using density functional theory (B3LYP) with a 6-31G(d) basis set. The value of $E_f - E_{HOMO}$ is calculated using the average work function of the two contacts of 4.6 eV (see Figure S-12; PPF = 5.0 and Si = 4.2) in order to approximate the value in a completed junction.

| Molecule | HOMO (eV) | LUMO (eV) | $E_f$ - $E_{HOMO}$ (eV) |
|---|---|---|---|
| NAB | -6.655 | -3.035 | 2.055 |
| AB | -6.118 | -2.168 | 1.518 |
| Octane | -8.03 | 2.48 | 3.43 |
| Hexylamine | -6.204 | 2.313 | 1.604 |
| Octylamine | -6.204 | 2.313 | 1.604 |
| Decylamine | -6.204 | 2.313 | 1.604 |
| Dodecylamine | -6.204 | 2.313 | 1.604 |

## References

1.  A. M. Mahmoud, A. J. Bergren and R. L. McCreery, *Anal. Chem.*, 2009, **81**, 6972-6980.
2.  A. M. Nowak and R. L. McCreery, *J. Am. Chem. Soc.*, 2004, **126**, 16621-16631.
3.  A. M. Nowak and R. L. McCreery, *Anal. Chem.*, 2004, **76**, 1089-1097.
4.  A. J. Bergren, K. D. Harris, F. Deng and R. L. McCreery, *J. Phys.: Condens. Matter*, 2008, **20**, 374117.
5.  A. J. Bergren, R. L. McCreery, S. R. Stoyanov, S. Gusarov and A. Kovalenko, *J. Phys. Chem. C*, 2010, **114**, 15806-15815.
6.  H. Yan and R. L. McCreery, *ACS Applied Materials & Interfaces*, 2009, **1**, 443-451.
7.  W. N. Hansen and G. J. Hansen, *Surface Science*, 2001, **481**, 172-184.
8.  R. Kumar, H. S. Mavi and A. K. Shukla, *Silicon*, 2010, **2**, 25.
9.  R. Shuker and R. W. Gammon, *Phys. Rev. Lett.*, 1970, **25**, 222-225.
10. J. E. Smith, Jr., M. H. Brodsky, B. L. Crowder, M. I. Nathan and A. Pinczuk, *Phys. Rev. Lett.*, 1971, **26**, 642.
11. R. J. Hemley, H. K. Mao, P. M. Bell and B. O. Mysen, *Phys. Rev. Lett.*, 1986, **57**, 747-750.
12. J. Heitmann, F. Muller, M. Zacharias and U. Gosele, *Adv. Mater.*, 2005, **17**, 795.
13. K. P. Jain, A. K. Shukla, S. C. Abbi and M. Balkanski, *Phys. Rev. B*, 1985, **32**, 5464.
14. D. Kovalev, H. Heckler, G. Polisski and F. Koch, *Phys. Stat. Sol. (B)*, 1999, **215**, 871.
15. A. K. Shukla and K. P. Jain, *Phys. Rev. B*, 1986, **34**, 8950-8953.
16. J. Zi, K. Zhang and X. Xie, *Phys. Rev. B*, 1997, **55**, 9263-9266.
17. H. S. Mavi, A. K. Shukla, R. Kumar, S. Rath, B. Joshi and S. S. Islam, *Semocond. Sci. Technol.*, 2006, **21**, 1627-1632.
18. B. G. Streetman and S. K. Banerjee, *Solid State Electronic Devices*, Prentice-Hall, Inc., Upper Saddle River, New Jersey, USA, 2009.
19. D. He, N. Okada and I. Shimizu, *Solar Energy Materials and Solar Cells*, 1994, **34**, 271-276.
20. J. Singh, ed., *Optical Properties of Condensed Matter and Applications*, John Wiley & Sons, New York, 2006.